PERGAMON

International Journal of Multiphase Flow 28 (2002) 1411–1435

International Journal of Multiphase Flow

www.elsevier.com/locate/ijmulflow

Investigation of two-phase flow pattern, void fraction and pressure drop in a microchannel

A. Kawahara [a,b], P.M.-Y. Chung [a], M. Kawaji [a,*]

[a] *Department of Chemical Engineering and Applied Chemistry, University of Toronto, 200 College Street, Toronto, Ont., Canada M5S 3E5*

[b] *Department of Mechanical Engineering and Materials Science, Kumamoto University, Kumamoto, 860-8555 Japan*

Received 5 March 2002; received in revised form 19 May 2002

Abstract

An experimental investigation has been carried out on two-phase flow characteristics in a 100 μm diameter circular tube. Two-phase flow patterns were determined by video recording the flow in the transparent capillary tube made of fused silica, in which de-ionized water and nitrogen gas were injected at superficial velocities of $j_G = 0.1$–60 m/s for gas, and $j_L = 0.02$–4 m/s for liquid. Time-averaged void fraction and two-phase friction pressure drop data were also obtained and analyzed. The flow patterns observed were intermittent and semi-annular flows, but a closer study of the liquid film structure revealed gas core flows with a smooth or ring-shaped film and a serpentine-like gas core surrounded by a deformed liquid film. Bubbly and churn flow patterns were not observed. A flow pattern map was developed based on the probability of appearance of each type of flow, and compared to the existing flow pattern maps obtained for ~1-mm diameter channels. Void fraction remained low even at high gas flow rates, indicating large slip ratios and weak momentum coupling between the phases. The single-phase friction factor and two-phase friction multiplier data were shown to be in good agreement with the conventional correlations.

Keywords: Microchannel; Gas–liquid flow; Flow patterns; Void fraction; Pressure drop; Liquid film; Ring film; Capillary tube

* Corresponding author. Tel.: +1-416-978-3063; fax: +1-416-978-8605.
E-mail address: kawaji@ecf.utoronto.ca (M. Kawaji).

0301-9322/02/$ - see front matter
PII: S0301-9322(02)00037-X

1. Introduction

Rapid development of microfluidic devices has triggered the demand for a comprehensive understanding of the flow characteristics in microchannels to advance their design and process control (Ho and Tai, 1998). Microscale devices can be fabricated using micromachining technologies and used for cooling microelectronic circuits, bioengineering applications, aerospace and microheat pipes, among others. Some of these applications involve gas–liquid two-phase flows in channels much less than 1 mm in diameter. The two-phase flow characteristics that need to be well understood include the two-phase flow regimes, void fraction and pressure drop. Although many theories, models and correlations have been developed for two-phase flow in relatively large diameter tubes, their applicability to microchannels also needs to be clarified.

There are many recent publications dealing with the two-phase flow characteristics in capillary tubes with a hydraulic diameter of about 1 mm (Bi and Zhao, 2001; Lee and Lee, 2001a,b; Zhao and Bi, 2001a,b; Yang and Shieh, 2001; Chen et al., 2001; Garimella et al., 2001; Triplett et al., 1999a,b; Coleman and Garimella, 1999; Xu et al., 1999; Lin et al., 1999; Ide et al., 1997; Mishima and Hibiki, 1996; Keska and Fernando, 1994; Fukano and Kariyasaki, 1993; Barajas and Panton, 1993; Lin et al., 1991; Damianides and Westwater, 1988; Suo and Griffith, 1964; among others), but few are yet available for channels with a diameter less than 100 μm.

With an order-of-magnitude reduction in the hydraulic diameter of the flow channel from 10 mm to 1 mm, significant differences have been reported in the two-phase flow pattern map, void fraction and pressure drop (see Kawaji, 1999 for a summary). In narrow channels, the gravitational effect is diminished so that the channel orientation no longer has a significant effect on the two-phase flow map. A low channel height results in the disappearance of a stratified flow pattern, and some of the flow pattern transition boundaries are also shifted. Void fraction and friction multiplier data can be correlated by conventional models, such as a drift flux model and the Lockhart–Martinelli correlation, but require some adjustments in the constants (Ali et al., 1993).

For another order-of-magnitude reduction in the channel diameter from ~1 mm to ~100 μm, further changes in the two-phase flow characteristics are expected. However, little information is yet available on microchannel two-phase flow. Stanley et al. (1997) used square and rectangular aluminum channels with hydraulic diameters, D_H, ranging from 56 to 256 μm to investigate single-phase and two-phase pressure drop and heat transfer. They used water and argon, helium and nitrogen gas to vary the viscosity, density and surface tension of their fluid system. They found that the available semi-empirical correlations for two-phase pressure drop substantially over predicted their data.

Feng and Serizawa (1999, 2000) and Serizawa and Feng (2001) conducted air–water and steam-water two-phase flow experiments in 25 and 50 μm capillary tubes and reported the observation of a liquid ring flow pattern, unique to flow channels of these dimensions. With an increase in the gas flow rate, the liquid bridge between two consecutive gas slugs became unstable and a transition from slug flow to liquid ring flow was observed. This flow pattern has not previously been observed in capillary tubes of 1 mm in diameter.

In single-phase flow through microchannels with diameters of the order of 10–100 μm, there have been reports of an early transition from a laminar to turbulent flow, and possible deviations of friction factors from conventional correlations, due to electrokinetic or surface charge effects and wall roughness (Kawaji et al., 2001). Feng and Serizawa's (1999, 2000) observation of a ring

flow pattern and Stanley et al.'s (1997) results also suggest that there may be significant differences in not only the two-phase flow regimes but also void fraction and pressure drop characteristics between microchannels with $D_H = 10$–100 μm and mini-channels with $D_H \sim 1$ mm.

Thus, the objectives of this work were to experimentally investigate the two-phase flow characteristics in a circular microchannel of 100 μm diameter, and identify the changes that occur due to a reduction in the channel diameter from ~1 mm to 100 μm. Since a smaller channel diameter automatically translates to lower Reynolds numbers and greater effects of wall shear and surface tension, this investigation is focused on a detailed study of the two-phase flow structures by flow visualization, followed by the development of a two-phase regime map and correlations of the void fraction and friction pressure drop data as presented below.

2. Experimental apparatus and procedure

2.1. Experimental apparatus

The experimental apparatus used in this work is shown in Fig. 1. A pneumatic pump was used to force the liquid through a microchannel test section at a constant flow rate. The pump was constructed from a pressure vessel filled with de-ionized water and connected to a nitrogen gas cylinder. To allow comparisons of the single-phase flow pressure drop data with those available in the literature, de-ionized water was chosen for the liquid phase. All the tubing and connections were made of stainless steel or brass to avoid any expansion of the flow loop volume under pressure.

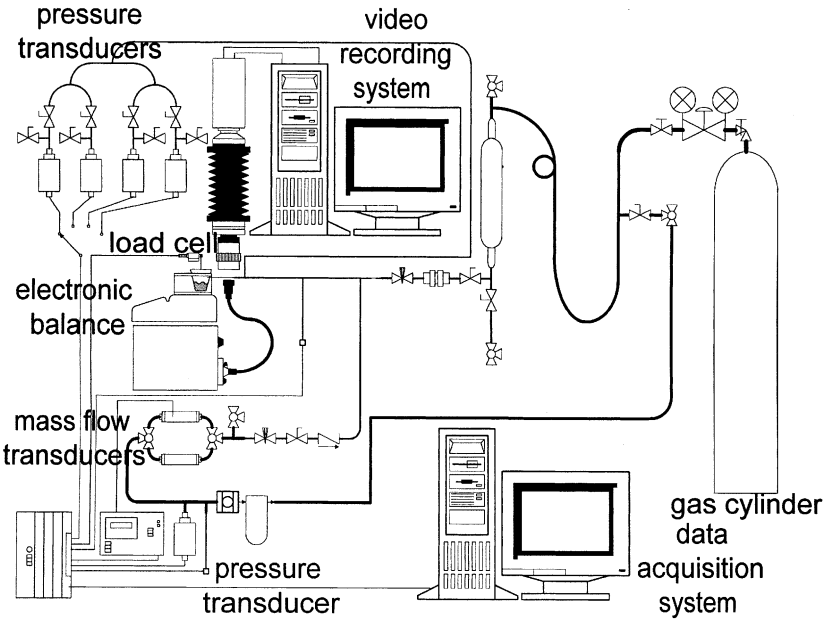

Fig. 1. Experimental apparatus.

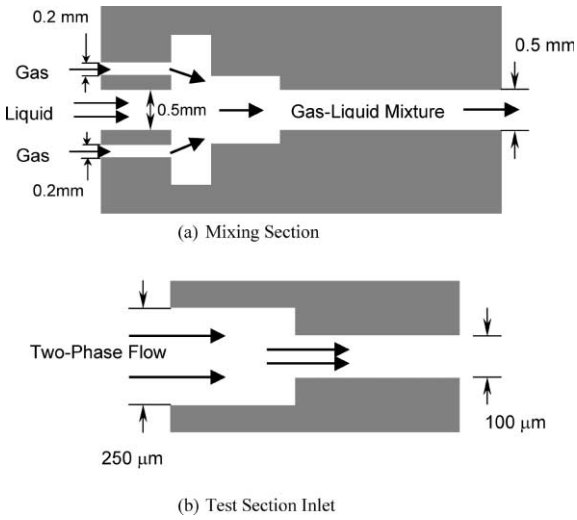

Fig. 2. Schematics of mixing section and test section inlet.

The test section was a circular transparent channel made of fused silica with an internal diameter of 100 μm and length of 64.5 mm, providing an L/D ratio of 645. The internal diameter was determined by imaging the channel cross-section using a microscope. The test section was placed horizontally and the inlet was connected to a tee junction with an internal diameter of 250 μm as shown in Fig. 2. The pressure in the tee junction was measured by one of four pressure transducers covering different ranges (200 ± 0.5 kPa, $1,374 \pm 13.7$ kPa, $3,435 \pm 8.6$ kPa, $13,740 \pm 34$ kPa). They were used to measure the pressure drop between the microchannel inlet and outlet, which included a minor loss due to a sudden contraction from 250 (tee junction diameter) to 100 μm. The liquid was discharged freely from the microchannel, so the outlet pressure was atmospheric. A thermocouple probe provided the fluid temperature upstream of the channel.

The liquid flow rate was measured by collecting in a small container the liquid discharged from the test section outlet over a sufficient period of time and measuring its weight using a load cell (50.97 ± 0.255 g). The nitrogen gas flow rate was measured using two mass flow meters (Matheson Instruments, Model 8172) with ranges of 0–10 and 0–50 SCCM. As shown in Fig. 2, the nitrogen gas was mixed with the liquid in a mixing section, which consisted of a 0.5 mm diameter internal passage for liquid and an external annular passage with a 0.2 mm gap for gas. The two streams would then mix by flowing into a 0.5 mm tube to which a tee junction with an internal diameter of 250 μm was connected for pressure measurement upstream of the test section. All analog signals for pressure, temperature and mass flow rate readings were recorded with a 16-bit data acquisition system at 100 samples per second.

Visualization of two-phase flow regimes in circular microchannels presented some challenges due to several factors: a limited amount of light that can pass through the test section and reach the video camera, a need to greatly magnify the image, and significant optical distortion. To observe the gas–liquid interface shape inside the microchannel, a 5× microscope objective was coupled to a monochrome CCD camera as shown in Fig. 1 that operated at a frame rate of 30 fps and a shutter speed of $1/16,000$ s. Background illumination was provided by a cold lamp and

gooseneck light guide placed behind the test section. To achieve the best background lighting condition, adjustments were made to the gain on the video camera. Images were captured from the digital video signal and saved onto a computer using a frame grabber and real-time video recording software. The contrast of the captured images was enhanced to improve the visibility of the gas–liquid interface.

To obtain undistorted images of two-phase flow inside a circular tube, an optical correction box is needed to minimize the beam steering effect of the curved tube wall and differences in refractive indices between the fluid and tube wall material. Optical distortion is a significant problem for flow visualization in circular microchannels because of the extremely small radii of wall curvature involved. For flow regime identification, it is also necessary to view a relatively long section of the channel, e.g., $L/D = 10$, so that the axial variations in the interfacial configuration can be determined. Too high a magnification can shorten the axial length of the view field, so the magnification must be adjusted until a suitable length of the test section is captured in the view field. In the present work, the view field length was set at $\sim$1 mm, so that the L/D ratio of the view field was $\sim$10.

To assess the optical distortion effect in the present channel, images of two-phase flow in the test section were recorded by the same video imaging system with and without the optical correction box filled with a refractive index-matched liquid. As shown in Fig. 3, the inner diameter of the microchannel was enlarged by about 50% without an optical correction box, although the same axial distance was captured. Thus, optical distortion has a magnifying effect only in the radial direction, especially near the channel walls, without affecting the axial view of the test section.

This result was utilized in the present experiments to better visualize the interfacial characteristics near the channel wall. When two-phase flow images were captured with the optical correction box, the liquid films could not be properly identified and studied for their structure. When the correction box was removed, the near wall region was magnified and the details of the liquid film such as the thickness variation along the channel wall could be better investigated. Of course, the liquid film thickness captured without the optical correction box would be significantly greater than the actual film thickness due to the optical distortion effect, so an appropriate correction must be applied if quantitative analyses of those images are to be performed.

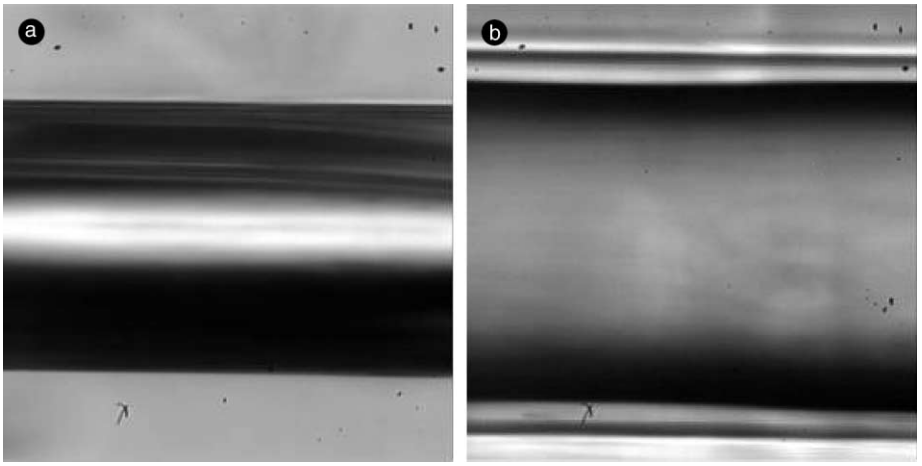

Fig. 3. Images of a gas core surrounded by a liquid film: (a) with and (b) without an optical correction box.

2.2. Reduction of pressure drop data

2.2.1. Friction pressure drop for single-phase liquid flow

For the circular microchannel used in the present study, single-phase flow experiments were first conducted to determine the friction factor using de-ionized water. The friction factor data were then compared with the conventional values for laminar flow in a circular channel.

If P_2 is the atmospheric pressure at the outlet of the microchannel and P_1 is the pressure measured by a pressure transducer at the inlet tee section, the pressure drop in the microchannel over the fully developed flow region, ΔP_{f2}, would be given by

$$\Delta P_{f2} = P_1 - P_2 + \frac{\rho}{2}(u_1^2 - u_2^2) - \Delta P_{f1} - \Delta P_{inlet} - \Delta P_{entrance}, \tag{1}$$

where ΔP_{f1} is the frictional pressure drop in the tee, ΔP_{inlet} is the pressure loss due to sudden contraction at the microchannel inlet, $\Delta P_{entrance}$ is the pressure drop in the entrance region, and u_1 and u_2 are the mean velocities in the tee section and microchannel, respectively.

The pressure drop in the sudden contraction is given by

$$\Delta P_{inlet} = K\frac{\rho u_2^2}{2}, \tag{2}$$

where K is the contraction coefficient assumed to be equal to 0.5 for the present channel. The pressure drop in the developing flow region is evaluated from

$$\Delta P_{entrance} = \zeta\frac{\rho u_2^2}{2}, \tag{3}$$

where the coefficient, ζ, is nearly equal to 1.31 according to Schmidt and Zeldin (1969). The length of the entry region ranged from about 0.01 to 18 mm depending on the Reynolds number. The mean velocities are given by

$$u_1 = \frac{m}{\rho A_1} \tag{4}$$

and

$$u_2 = \frac{m}{\rho A_2}, \tag{5}$$

where m is the mass flow rate and A_1 and A_2 are the cross-sectional areas of the tee section and the microchannel, respectively.

The Darcy friction factor for the microchannel, f_D, is calculated from

$$f_D = \frac{\Delta P_{f2}}{\Delta L}\frac{2D_H}{\rho u_2^2}, \tag{6}$$

where D_H is the hydraulic diameter and ΔL is the length of the microchannel. The values obtained will be compared with the conventional laminar friction factor for a circular channel,

$$f_D = \frac{64}{Re}. \tag{7}$$

The Reynolds number is calculated based on the hydraulic diameter:

$$Re = \frac{GD_H}{\eta}, \tag{8}$$

where G is the mass flux and η is the dynamic viscosity.

2.2.2. Frictional pressure drop for two-phase flow

The overall pressure drop measured in horizontal two-phase flow, $\Delta P_{measured}$, is given by

$$\Delta P_{measured} = \Delta P_{friction} + \Delta P_{contraction} + \Delta P_{acceleration}, \tag{9}$$

where $\Delta P_{friction}$ is the pressure drop due to wall friction, $\Delta P_{contraction}$ is the pressure loss due to contraction from the tee into the microchannel, and $\Delta P_{acceleration}$ is the pressure change due to acceleration. In order to obtain two-phase friction pressure drop data, the second and third terms on the right hand side of Eq. (9) must be estimated and subtracted from the total two-phase pressure drop measured. Thus, $\Delta P_{contraction}$ was estimated using a homogeneous flow model recommended in some references (e.g., Collier, 1972; Hewitt et al., 1993):

$$\Delta P_{contraction} = \frac{G^2}{2\rho_L}\left[\left(\frac{1}{C_C} - 1\right)^2 + 1 - \gamma^2\right]\left[1 + x\left(\frac{\rho_L}{\rho_G} - 1\right)\right], \tag{10}$$

where G is the total mass flux of both gas and liquid ($= G_G + G_L$), x is the mass flow quality, ρ_G and ρ_L are the respective densities of gas and liquid, γ is the ratio of the cross-sectional area in the tee to that in the test section, C_C is the coefficient of contraction which is a function of the area ratio. The latter coefficient was estimated from the following equation proposed by Chisholm (1983):

$$C_C = \frac{1}{0.639(1-\gamma)^{0.5} + 1}. \tag{11}$$

The pressure drop due to acceleration was estimated using the following expression:

$$\Delta P_{acceleration} = \left[\frac{G^2x^2}{\rho_G\varepsilon} + \frac{G^2(1-x)^2}{\rho_L(1-\varepsilon)}\right]_{outlet} - \left[\frac{G^2x^2}{\rho_G\varepsilon} + \frac{G^2(1-x)^2}{\rho_L(1-\varepsilon)}\right]_{inlet}, \tag{12}$$

where ε is the time-averaged void fraction. In this study, the void fraction was evaluated using the following empirical correlation:

$$\varepsilon = \frac{0.03\beta^{0.5}}{1 - 0.97\beta^{0.5}}, \tag{13}$$

where β is the homogeneous void fraction [$= j_G/(j_G + j_L)$]. Eq. (13) was developed from the void fraction data obtained in the present circular microchannel as discussed in the next section. In Eqs. (12) and (13), the void fractions and superficial gas velocities at the microchannel inlet and outlet were calculated using the nitrogen gas density evaluated at the channel inlet and outlet pressures.

Fig. 4 shows the components of pressure drop due to inlet contraction and acceleration calculated using Eqs. (10) and (12), respectively. In the present microchannel, the contributions of

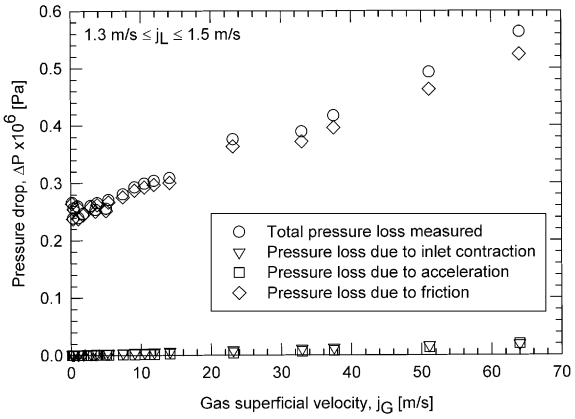

Fig. 4. Components of total two-phase pressure drop in a circular microchannel.

inlet contraction and acceleration were found to range from 0.05% to 9% and 0% to 4.5%, respectively, of the total pressure drop depending on the flow conditions.

2.3. Evaluation of superficial gas velocity and gas density

All experiments were conducted at room temperature and under atmospheric pressure at the microchannel outlet. The static pressure varied axially from the inlet to the outlet as indicated by the total pressure drop data shown in Fig. 4, so the gas density also varied considerably along the microchannel, while the change in liquid density was insignificant. Since superficial gas and liquid velocities are commonly used to present various measurements, the gas density had to be evaluated using the appropriate pressure. For the pressure drop data, the average pressure between the microchannel inlet and outlet was used, while the local pressure at the observation window was used for flow regime and void fraction data. Both pressures were obtained assuming a linear variation of pressure along the microchannel.

To verify the validity of a linear pressure profile assumption, a numerical calculation was performed using the void fraction and two-phase friction multiplier correlations developed in this work. The microchannel length was divided into many short segments, and the pressure drop, gas density and superficial gas velocity in each segment were calculated in an iterative manner to arrive at the atmospheric pressure at the channel outlet. From these calculations, the assumption of an axially linear pressure distribution was found to be valid. Non-linear pressure distribution could be obtained if compressibility effects become significant. But, even at the highest nitrogen gas flow rate tested, the Mach number based on the sound of speed in nitrogen gas was well below 0.3, typical of incompressible flow. Thus, the effect of compressibility was considered to be insignificant.

2.4. Measurement uncertainty

The maximum uncertainties in the gas and liquid flow rates, superficial velocities, void fraction, total two-phase pressure gradient, two-phase frictional pressure gradient and two-phase friction

Table 1
Measurement uncertainties

Parameters	Uncertainty range
Mass flow rate of liquid, m_L	±0.1% to ±1%
Mass flow rate of gas, m_G	±1% to ±10%
Superficial liquid velocity, j_L	±2.1% to ±3%
Superficial gas velocity, j_G	±3% to ±12%
Void fraction, ε	−0.05 to −0.01
Total two-phase pressure gradient, $(\Delta P/\Delta Z)$	±1% to ±4%
Two-phase frictional pressure gradient, $(\Delta P_f/\Delta Z)_{TP}$	±2% to ±7%
Two-phase friction multiplier, ϕ_L^2	±2% to ±7%

multiplier were estimated using a propagation of error analysis and are summarized in Table 1. The uncertainties changed depending on the flow conditions, so their ranges from minimum to maximum are shown in Table 1.

3. Results and discussion

3.1. Two-phase flow regime

Fig. 5 shows typical images of two-phase flows observed in the present circular microchannel at different gas flow rates and a low liquid flow rate (Fig. 5a), medium liquid flow rate (Fig. 5b), and high liquid flow rate (Fig. 5c). At a given flow condition, different flow patterns were observed which can be classified into five distinctive patterns depending on the interfacial configuration: "liquid alone (or liquid slug)", "gas core with a smooth-thin liquid film", "gas core with a smooth-thick liquid film", "gas core with a ring-shaped liquid film" and "gas core with a deformed interface".

The "liquid alone" pattern showed no entrained bubbles or gas–liquid interface in the 1-mm long view field, and appeared under all conditions. Smooth liquid films surrounding the gas core could be characterized as either thin or thick, and wavy liquid films were classified as ring-shaped or deformed. The ring-shaped liquid films appear to be unique to microchannels as first reported by Feng and Serizawa (1999, 2000) in 25- and 50-μm diameter capillary tubes. In the present work, the interval between neighboring liquid rings was found to vary within a given flow condition as well as for different flow conditions. The ring-shaped liquid films and smooth-thin liquid films were both axi-symmetrically distributed around the channel inner wall, indicating the effect of gravity on the two-phase flow pattern is negligible in microchannels as previously pointed out by Serizawa and Feng (2000).

At medium and high liquid flow rates, a gas flowing in the core surrounded by a smooth-thick liquid film or deformed interface film was observed in addition to gas core flows with a smooth-thin or ring-shaped liquid film. The thickness of the liquid film sometimes exceeded the diameter of the gas core. The shape and motion of the deformed interface film resembled a serpentine-like gas core moving through the tube and, to our knowledge, this type of flow pattern has not been previously observed in gas–liquid two-phase flows in small or large flow channels. It is similar to a

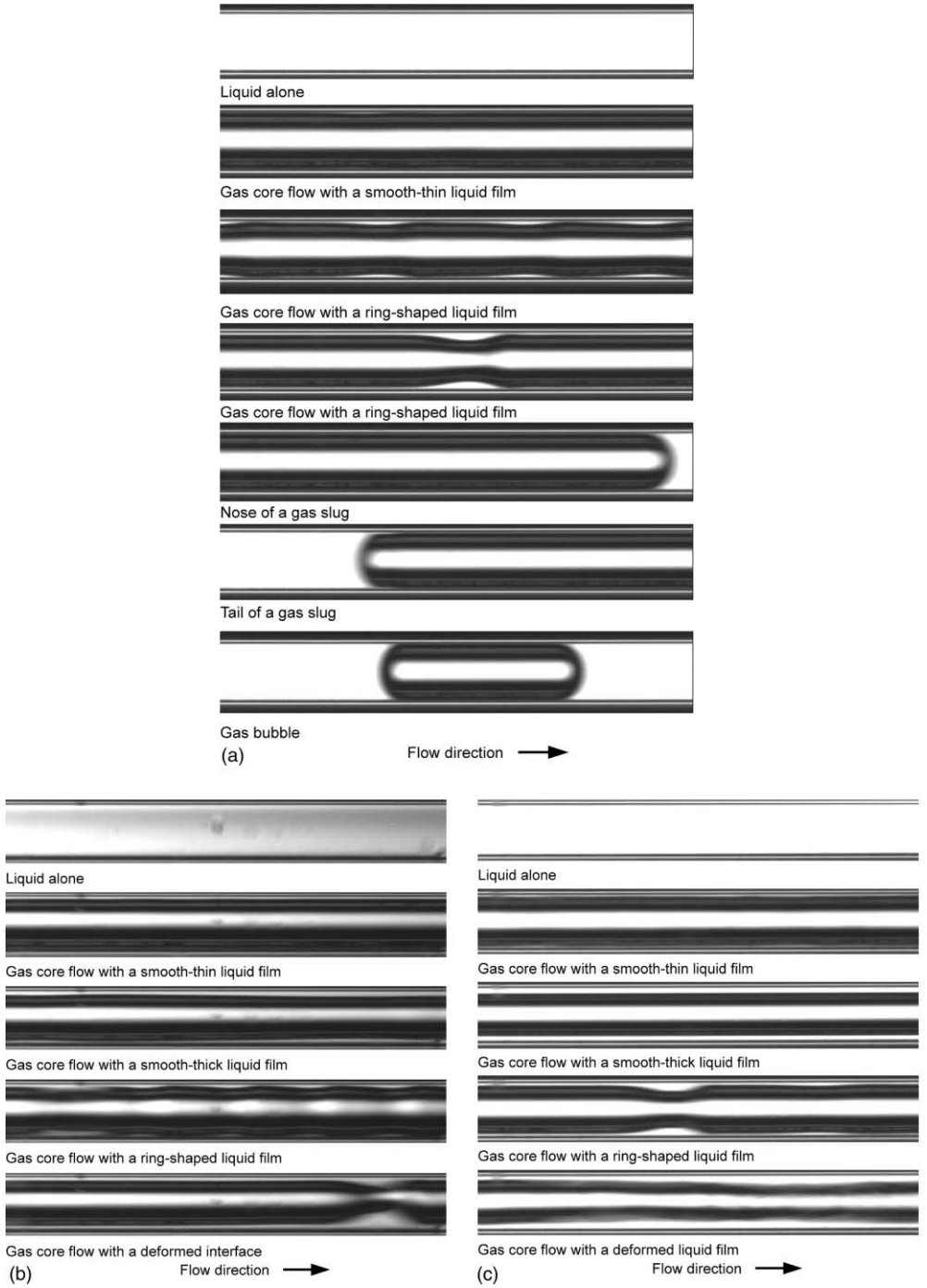

Fig. 5. Images of two-phase flow in a microchannel (a) at low liquid and intermediate gas flow rates ($j_L = 0.15$ m/s, $j_G = 6.8$ m/s), (b) at intermediate liquid and high gas flow rates ($j_L = 0.56$ m/s, $j_G = 20.3$ m/s), (c) at high liquid and gas flow rates ($j_L = 3.96$ m/s, $j_G = 19.0$ m/s).

flow pattern called "disturbed core-annular" or "corkscrew core flow" occurring in liquid–liquid flows (Joseph et al., 1997).

For all the flow conditions tested in this study, a bubbly flow pattern with bubbles much smaller than the channel diameter (100 μm) was never observed. Although a gas bubble is shown in Fig. 5a, it is a gas plug rather than a spherical bubble, with a volume-equivalent diameter much greater than the channel diameter of 100 μm. While liquid only flows (or liquid slugs) containing small spherical bubbles were not observed, small droplets were observed inside gas core flows. Furthermore, no stratified flow occurred in the present microchannel as reported in previous studies of two-phase flow patterns in channels with a diameter close to 1 mm (Damianides and Westwater, 1988; Fukano and Kariyasaki, 1993; Triplett et al., 1999b; Zhao and Bi, 2001a).

In developing a two-phase flow pattern map for the present microchannel, it became clear that new flow patterns need to be defined to fully describe the flow characteristics obtained in this work, because of the simultaneous occurrence of different flow patterns in the channel under any given flow condition as shown in Fig. 5. Thus, the time fractions of different flow patterns were obtained for each two-phase flow condition, as typically shown in Figs. 6 and 7 for low and high liquid flow rates, respectively. In the case of a low liquid flow rate (Fig. 6), three flow patterns alternately appeared at the observation section of the microchannel: (A) liquid alone, (B) gas core with a smooth-thin liquid film and (C) gas core with a ring-shaped liquid film. At high liquid flow rates (Fig. 7), two additional flow patterns were observed in addition to the three above: (D) gas core with a smooth-thick liquid film, and (E) a serpentine-like gas core with a deformed liquid film. The number of images containing each flow pattern was then counted and the probability of appearance was computed for a given flow condition. Based on these probabilities and the time-averaged void fraction for each flow condition, four flow regimes were defined as follows:

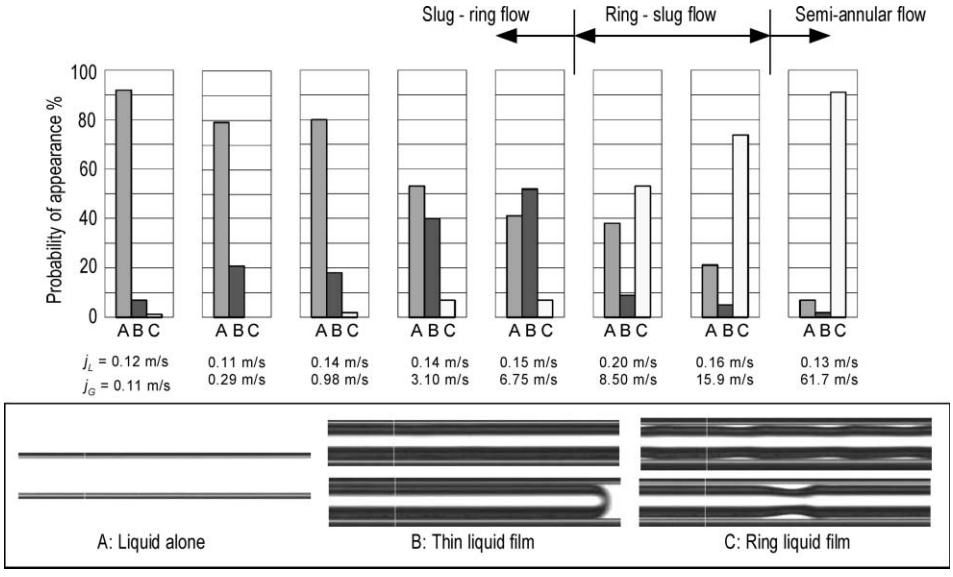

Fig. 6. Probability of appearance of different two-phase flow patterns at low liquid flow rates.

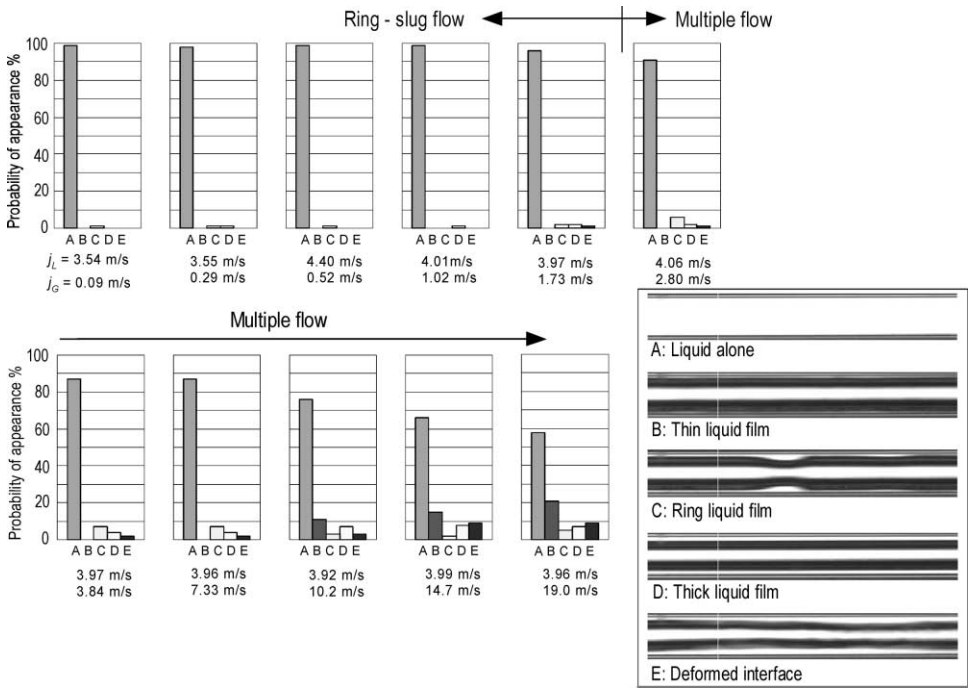

Fig. 7. Probability of appearance of different two-phase flow patterns at high liquid flow rates.

- "Slug-ring flow" is the flow in which the probability of B is larger than that of C and the time-averaged void fraction is less than 0.8.
- "Ring-slug flow" is the flow in which the probability of C is greater than that of B and the time-averaged void fraction is less than 0.8.
- "Semi-annular flow" is the flow in which the flow alternates mostly between A and C. The time-averaged void fraction is greater than 0.8.
- "Multiple flow" contains all five flow patterns, A–E, and the time-averaged void fraction is less than 0.8.

At a low superficial liquid velocity (Fig. 6), a "liquid alone" flow pattern was predominantly occurring more than 80% of the time at a given location at low superficial gas velocities ($j_G < 1$ m/s). As the gas flow rate was increased, the occurrence of "liquid alone" flow decreased, falling to 50% probability at $j_G = 6.75$ m/s, and less than 5% at $j_G = 15.9$ m/s. On the other hand, a gas core flow with a smooth-thin liquid film quickly increased its probability of occurrence, reaching a maximum probability of 50% at $j_G = 6.75$ m/s, but decreased thereafter with increasing gas flow. The probability of a gas core flow with a ring-shaped film increased very slowly with j_G below 6.75 m/s, but started to increase suddenly at $j_G = 8.5$ m/s and reached over 90% at $j_G = 61.7$ m/s. Thus, with an increase in the gas flow rate, the predominant flow pattern at low liquid flow rates changed from a "liquid alone" flow to a "gas core flow with a smooth-thin liquid film", and finally to a "gas core flow with a ring-shaped liquid film".

At high liquid flow rates, a gas core flow with a smooth-thick liquid film and a serpentine-like gas core flow with a deformed film were additionally observed as shown in images D and E in Fig. 7, respectively. The probability of a "liquid alone" flow remained high at above 80% for $j_G < 10$ m/s, and over 50% even at $j_G = 19$ m/s. Among the aforementioned flow patterns, gas core flows with a smooth-thin liquid film and ring-shaped film appeared at low gas flow rates ($j_G < 1$ m/s), but the deformed film was not observed until j_G reached 1.7 m/s. At $j_G > 2.8$ m/s, all five flow patterns appeared, but the ring-shaped film decreased its probability of occurrence while the thin, thick and deformed films increased their probabilities with an increasing gas flow rate. Thick liquid films were observed without the use of an optical correction box, and this could be due to the magnification of images in the near-wall region. Although the exact film thickness is not easy to determine, the occurrence of thick liquid films was clearly limited to the high liquid flow rate runs. At high liquid and gas flow rates, every flow pattern, A, B, C, D and E, could be observed as shown in Fig. 7, and this was defined as the "multiple flow" regime. For this flow regime, the time-averaged void fraction was always less than 0.8.

Fig. 8 shows the overall two-phase flow regime map developed for the present microchannel. The ordinate and abscissa are the superficial velocities of liquid and gas, respectively, at the observation window. Here, the superficial gas velocity was calculated based on the gas density evaluated at the pressure in the observation area, which was determined by assuming a linear pressure variation between the channel inlet and outlet. In Fig. 8, the solid lines represent the boundaries at which flow regime transition occurred among the four flow patterns, i.e., slug-ring, ring-slug, multiple and semi-annular flows.

The present flow regime map can be compared with other maps developed previously for air–water two-phase flow in small-diameter horizontal and vertical channels. Fig. 9a–d show comparisons with the results of Damianides and Westwater (1988), Fukano and Kariyasaki (1993), Triplett et al. (1999b) and Zhao and Bi (2001a), respectively. The broken lines represent the flow regime transition boundaries observed in the ~1 mm diameter channels and the flow regime names in brackets are those given by the respective authors.

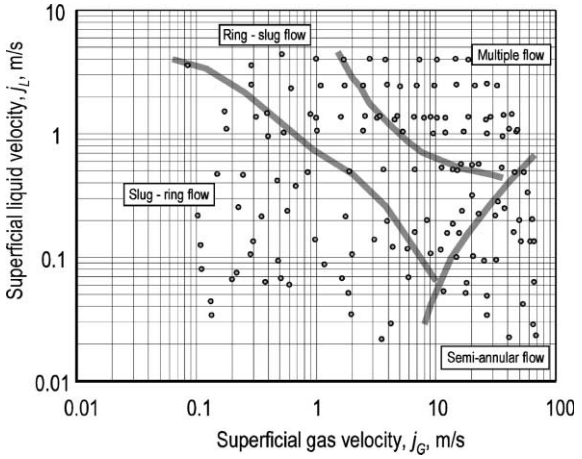

Fig. 8. Two-phase flow regime map for a 100 μm microchannel.

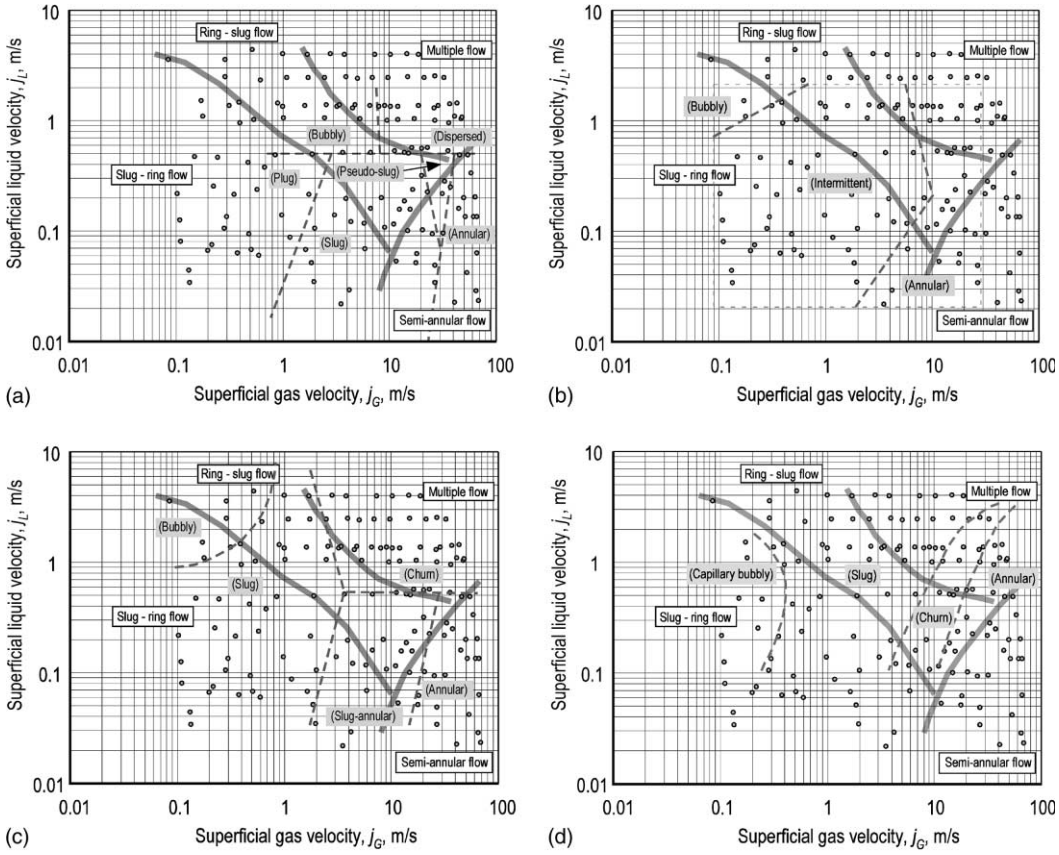

Fig. 9. Comparison of two-phase flow regime maps: (a) Damianides and Westwater (1988), (b) Fukano and Kariyasaki (1993), (c) Triplett et al. (1999b) and (d) Zhao and Bi (2001a).

Damianides and Westwater (1988) used a 1-mm inner diameter, circular horizontal channel, and identified five flow regimes, i.e., bubbly, plug, slug, pseudo-slug, dispersed and annular flows. Fukano and Kariyasaki (1993) identified three flow regimes, namely, bubby, intermittent and annular flows, in a horizontal capillary tube having a 1-mm inner diameter. Triplett et al. (1999b) distinguished five flow regimes in a horizontal circular channel having a 1.1-mm inner diameter: bubbly, slug, churn, slug-annular and annular flows. Most recently, Zhao and Bi (2001a) observed "capillary bubbly", slug, churn and annular flows in a vertical equilateral-triangular channel with a hydraulic diameter of 0.87 mm.

There are similarities and differences between the present and other flow regime maps obtained in ~1-mm diameter channels. While intermittent flow patterns such as plug and slug flow, and an annular (or semi-annular) flow pattern have been observed in both the present microchannel and ~1-mm diameter channels, bubbly and churn flow patterns are absent in the microchannel results. Differences in the locations of the transition boundaries are also found, but some variations already exist among the flow regime maps for ~1-mm diameter channels, so this aspect will not be pursued in detail. Instead, we will focus on the significant differences concerning the bubbly flow and multiple flow patterns. The multiple flow pattern has been observed for the first time in a

microchannel at high liquid and gas flow rates, with alternating occurrences of liquid alone and gas core flows with different liquid film geometries as illustrated in Fig. 7. In ~1 mm diameter channels, both Zhao and Bi (2001a) and Triplett et al. (1999b) observed a churn flow under the similar flow conditions instead. The churn flow involves a highly agitated gas–liquid interface, indicative of the high turbulence level in the two-phase mixture. Although slight interface deformation was observed in the serpentine-like gas core, the degree of interface deformation seen in the multiple flow pattern in the present microchannel is incomparably smaller than that obtained in churn flow.

The bubbly flow pattern always appears in larger channels typically at high liquid and low gas flow rates, due to turbulence in the liquid breaking up the gas phase into small bubbles. However, it was not observed at all in the 100 μm microchannel within the present flow conditions, even at high superficial liquid velocities up to 4 m/s. The lowest superficial gas velocity covered in the present work was ~0.1 m/s, and it may not be considered as sufficiently low for microchannels, since Serizawa and Feng (2001) showed images of very small bubbles and a chain of short bubbles in microchannels under certain conditions. Also, in flow boiling situations, small bubbles nucleating in a heated microchannel may be swept by high-speed liquid flow to form a bubbly flow pattern. However, conducting steady two-phase flow experiments at much lower superficial gas velocities, $j_G \ll 0.1$ m/s, involves some practical difficulties in the measurement of such extremely small volumes of gas continuously injected into the microchannel. The gas subsequently expands within the microchannel due to the large pressure drop, especially at high liquid flow rates.

In the present work, the absence of the bubbly and churn flow patterns may be mainly attributed to the laminar nature of the liquid flow in the microchannel, even at the highest superficial liquid velocity tested. For example, the liquid Reynolds number based on $j_L = 4$ m/s is only about 400 for water flowing through a 100 μm microchannel. Even with the injection of gas flow, not enough turbulence can be induced and sustained in the liquid to break up the gas phase into small bubbles with diameters less than the channel diameter. Thus, from a liquid turbulence point of view, the bubbly flow regime is not expected to occur in microchannels except at much higher superficial liquid velocities, possibly over 20 m/s, and sufficiently low gas velocities. This would mean that the frictional pressure drop would be so large that the bubbly flow regime could only occur over very short distances in the microchannels.

3.2. Void fraction

Void fraction in the present channel was estimated by analyzing the images of gas–liquid interfaces recorded in the observation window of the channel. Each image covered a distance of about 1 mm in the flow direction. At low liquid flow rates, most of the recorded images showed either liquid flowing alone ($\varepsilon = 0$) or a gas core flow with a smooth-thin liquid film or ring-shaped liquid film. For the latter flow pattern, the void fraction was assumed to be unity. By counting the number of images containing each flow type, the time-averaged void fraction was determined from the following expression:

$$\varepsilon = \frac{\text{Number of gas core images}}{\text{Total number of images counted}}. \tag{14}$$

On the other hand, at high liquid flow rates, three types of images were recorded: liquid flowing alone ($\varepsilon = 0$), a gas core flow with a thin liquid film or a ring-shaped film ($\varepsilon = 1$), and a gas core flow with a thick liquid film ($0 < \varepsilon < 1$). For the gas core with a thick liquid film, a gas core volume fraction, ε_{gc}, was estimated by regarding the gas core as a cylinder of a smaller radius than the channel radius. Then, the time-averaged void fraction for high liquid flow rates was determined using the following expression:

$$\varepsilon = \frac{\text{Number of images of gas core flows with a thin liquid film} + \sum \varepsilon_{gc}}{\text{Total number of images counted}}, \tag{15}$$

where the gas core volume fraction, ε_{gc}, was summed for all the images containing gas core flows with thick liquid films.

Since optical distortion effects were present, the void fractions for gas core flows with ring-shaped films and thick liquid films may have been somewhat underestimated. To check the degree of overestimation involved, void fraction was also calculated from images exhibiting a ring-shaped liquid film in several experimental runs without any optical distortion effects obtained by immersing the observation window of the microchannel into an optical correction box filled with a refractive index-matching liquid. For high superficial liquid velocity runs where the ring-film was the thickest, the estimated values of the void fraction ranged from 0.92 to 0.94 instead of unity. Given the low probabilities of occurrence (<10%) for both ring-shaped films and thick films at high liquid flow rates, however, neglecting the liquid film should not have caused a significant error in the time-averaged void fraction calculation.

At low superficial liquid velocities, where the occurrence of ring film was more frequent, the liquid ring protruded less and the actual void fraction was closer to unity. In addition, since the void fractions for gas core flows with thin liquid films were slightly overestimated due to the assumption of $\varepsilon = 1$, this overestimation would be compensated by the slight underestimation of the void fraction for gas core flows with thick films due to optical distortion effects. Thus, for all flow conditions tested, the neglect of liquid films in void fraction calculation was regarded to be an acceptable assumption causing little error.

Fig. 10 shows the time-averaged void fraction results for the present circular microchannel. The void fraction is plotted against a homogeneous void fraction, $\beta[= j_G/(j_G + j_L)]$, with different symbols used for different ranges of liquid superficial velocity, j_L. The superficial gas velocity at the observation window was estimated as explained in Section 2.3. It is clear that the void fraction is not strongly dependent on j_L, and can be correlated with the homogeneous void fraction. The solid curve in the figure is given by Eq. (13), which best fits the present void fraction data.

The time-averaged void fraction in the present microchannel remained low even for relatively high homogeneous void fractions, $\beta < 0.8$, but increased rapidly for $0.8 < \beta < 1$. The data and best fit curve are highly non-linear indicating strong deviations from linear relations for a homogeneous flow (i.e., $\varepsilon = \beta$, shown by a dotted line in Fig. 10) and two-phase flows in narrow rectangular channels. For the latter, Ali et al. (1993) and others have reported that the void fraction in narrow channels with $D_H \sim 1$ mm can be approximately given by an Armand-type (1946) correlation, $\varepsilon = 0.8\beta$, which is shown by a dashed line in Fig. 10.

The deviation from a linear relationship between ε and β can be attributed to several factors. A single-phase liquid flow pattern was observed most frequently at high liquid flow rates for all gas flow rates (Fig. 6), and at low liquid and gas flow rates (Fig. 7). Due to the wall shear and strong

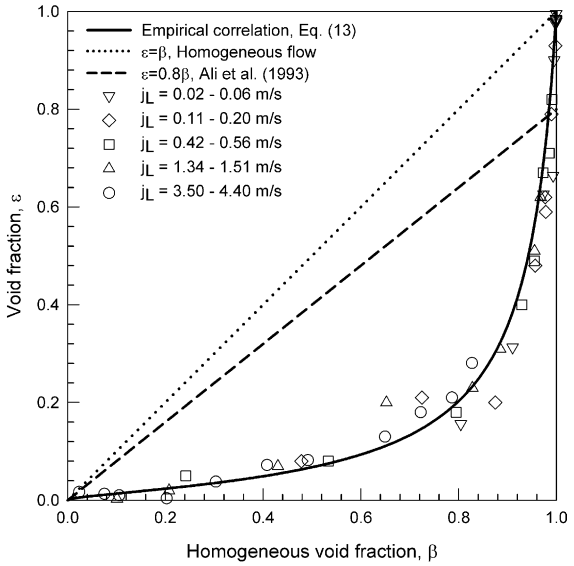

Fig. 10. Relation between measured and homogeneous void fractions.

surface tension effects, the slowly moving liquid often bridged the channel cross-section completely. The absence of gas phase in these liquid-only flow sections resulted in low time-averaged void fractions. On the other hand, at low liquid and high gas flow rates (Fig. 7), the two-phase flow pattern was mostly separated (i.e., a gas core surrounded by a liquid film) with weak momentum coupling between them. The liquid flow was strongly influenced by wall shear and surface tension, but the gas phase could flow unhindered in the channel core, unlike in larger channels where the interface is more deformed and the gas phase experiences much greater flow resistance and stronger momentum coupling with the liquid phase.

As a result of the unique flow characteristics mentioned above, the slip ratio in microchannels can be an order-of-magnitude higher than those in channels of D_H greater than ~1 mm, even at relatively low gas flow rates. For example, at $\beta = 0.5$ and 0.8, the void fraction is about 0.1 and 0.2, so the slip ratio, u_G/u_L, is ~9 and 16, respectively. On the other hand, if Ali et al.'s (1993) correlation, $\varepsilon = 0.8\beta$, is used, the slip ratio would be 1.4 and 2.0 at $\beta = 0.5$ and 0.8, respectively.

3.3. Pressure drop and friction factor in single-phase liquid flow

Prior to performing the two-phase flow experiments, single-phase pressure drop data were obtained using de-ionized water in the circular microchannel. The friction factor was determined from the measured pressure drop, $P_l - P_{atm}$, for a given mass flow rate, m, by using Eqs. (1)–(6) and neglecting the frictional pressure drop in the tee section containing the pressure transducer, i.e., $\Delta P_{fl} = 0$.

In Fig. 11, the friction factor data are plotted against the Reynolds number based on the hydraulic diameter. Below $Re = 1900$, the friction factor results show good agreement with the theoretical laminar correlation for a circular tube, which is indicated by a solid line. The present

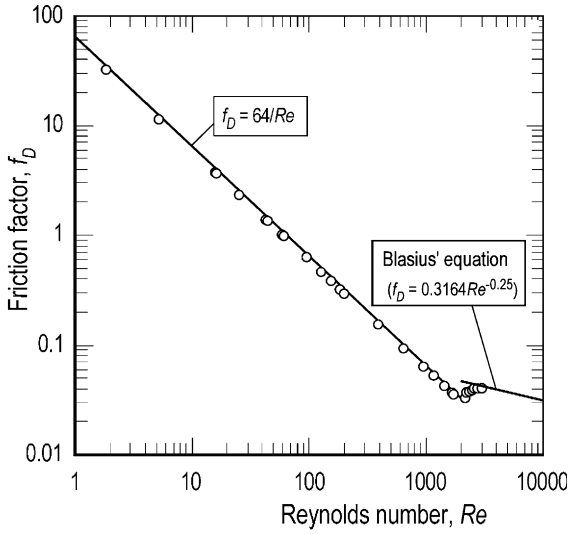

Fig. 11. Friction factor data for single-phase water flow.

data were, on the average, 6% below the conventional correlation, as the best-fit curve is given by the following equation:

$$f_{\mathrm{D}} = \frac{60.3}{Re}. \tag{16}$$

Fig. 11 also shows that the laminar-to-turbulent transition was found to occur at about $Re = 1900$–2000 in the present microchannel, which is essentially the same as in larger channels. For the analysis of two-phase friction pressure drop described below, the liquid Reynolds number was well below the critical Reynolds number, so Eq. (16) was used to calculate the single-phase friction pressure drop.

3.4. Two-phase frictional pressure drop

Fig. 12 presents typical two-phase frictional pressure gradient data obtained in the 100 μm circular microchannel. The data are plotted against the superficial gas velocity, j_{G}, for different superficial liquid velocities, j_{L}. The gas density at the average pressure between the microchannel inlet and outlet was used to evaluate the superficial gas velocity. As expected, the two-phase frictional pressure gradient increases with increasing j_{L} and j_{G}.

According to some previous studies on two-phase frictional pressure drop, the homogeneous flow model was shown to predict the data well; for example, for ammonia-steam flow in circular microchannels with $D = 1.46$–3.15 mm by Ungar and Cornwell (1992), and for air–water flow in circular and semi-triangular microchannels with hydraulic diameters $D_{\mathrm{H}} = 1.09$ and 1.49 mm by Triplett et al. (1999a). However, in the present microchannel, the two-phase flow patterns were much less homogeneous, as indicated by the video images and very large slip ratios presented in the previous sections. Thus, the homogeneous flow model may not be able to successfully correlate the present two-phase pressure drop data.

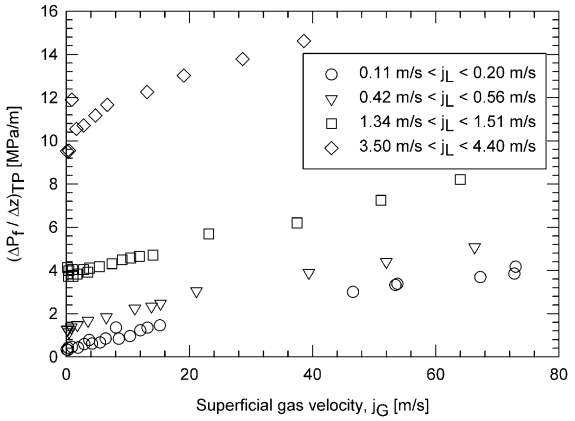

Fig. 12. Two-phase friction pressure gradient data.

In the homogeneous flow model, the two-phase pressure gradient, $(\Delta P_f/\Delta Z)_{TP}$, is calculated from,

$$\left(\frac{\Delta P_f}{\Delta Z}\right)_{TP} = f_{DH}\frac{1}{D}\frac{G^2}{2\rho_H}, \tag{17}$$

where ρ_H is the homogenous mixture density defined by,

$$\frac{1}{\rho_H} = \frac{x}{\rho_G} + \frac{1-x}{\rho_L} \tag{18}$$

and f_{DH} is the two-phase Darcy friction factor. This friction factor, f_{DH}, is a function of the homogeneous Reynolds number:

$$Re_H = \frac{GD}{\eta_H}, \tag{19}$$

where G is the total mass flux and η_H is the homogeneous mixture viscosity. Several models have been proposed to evaluate the two-phase mixture viscosity, and the model selected may affect the predicted two-phase frictional pressure drop (Wong and Ooi, 1995). Accordingly, the present experimental data are compared with the predictions of the homogeneous flow model, calculated using the following two-phase viscosity models:

Owens (1961): $$\eta_H = \eta_L, \tag{20}$$

McAdams (1954): $$\eta_H = \left(\frac{x}{\eta_G} + \frac{1-x}{\eta_L}\right)^{-1}, \tag{21}$$

Cicchitti et al. (1960): $$\eta_H = x\eta_G + (1-x)\eta_L, \tag{22}$$

Dukler et al. (1964): $$\eta_H = \beta\eta_G + (1-\beta)\eta_L, \tag{23}$$

Beattie and Whalley (1982): $$\eta_H = \eta_L(1-\beta)(1+2.5\beta) + \eta_G\beta, \tag{24}$$

Lin et al. (1991): $$\eta_H = \frac{\eta_L\eta_G}{\eta_G + x^{1.4}(\eta_L - \eta_G)}. \tag{25}$$

In Fig. 13, the present data are compared with the homogeneous flow model predictions using the different viscosity models given above. It is clear that the agreement between the experimental data and homogeneous flow model is generally poor, with reasonably good predictions (within ±20%) obtained only with Dukler et al.'s (1964) model for the mixture viscosity.

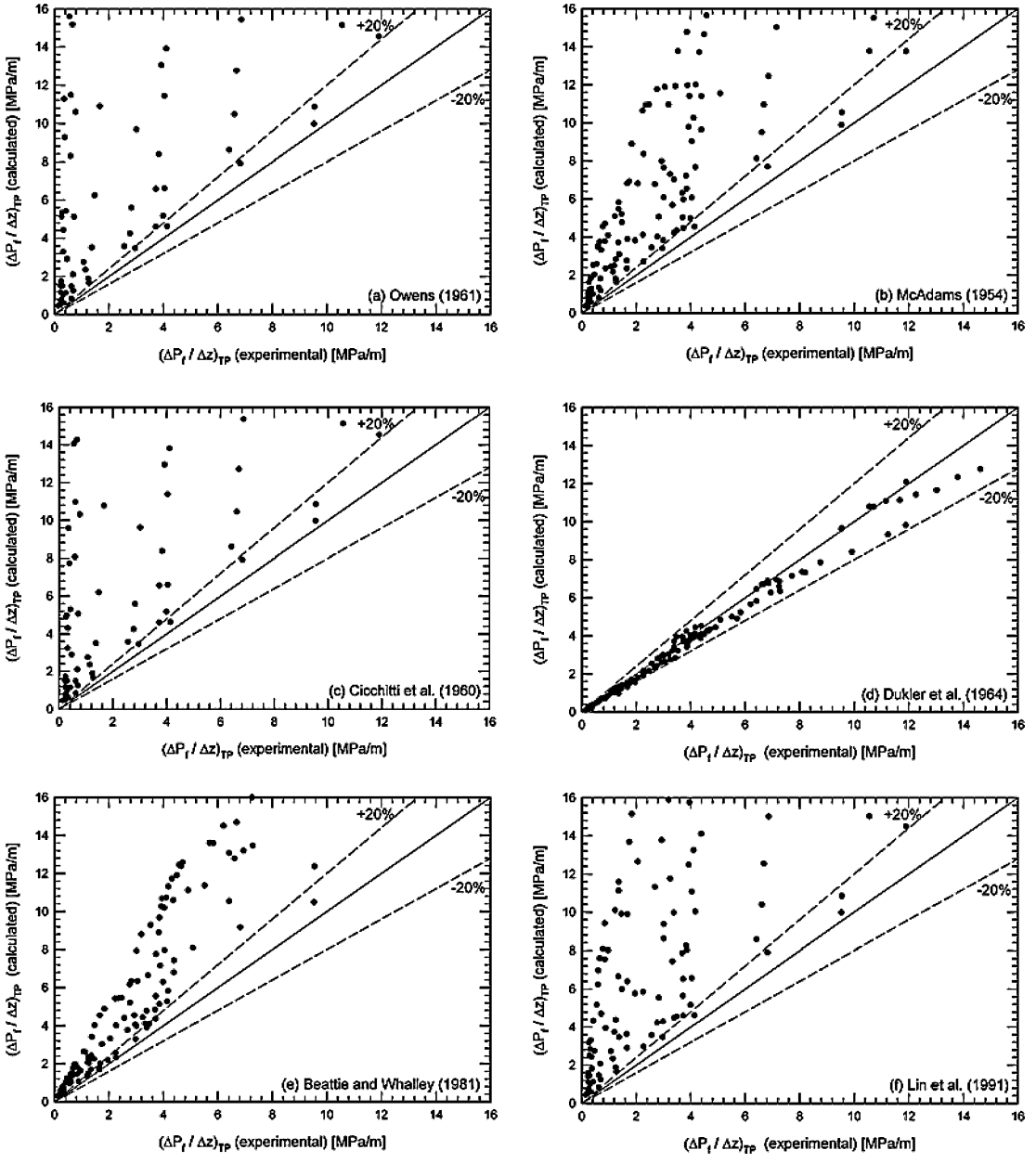

Fig. 13. Comparison of the two-phase frictional pressure gradient between microchannel data and homogeneous flow model predictions using different viscosity formulations.

On the other hand, the Lockhart and Martinelli (1949) correlation was developed based on a separated flow assumption, and has been found by Zhao and Bi (2001b) to represent their data reasonably well for vertical air–water flow in miniature triangular channels with $D_H = 0.87$–2.89 mm. The Lockhart and Martinelli (1949) correlation uses a two-phase friction multiplier, ϕ_L^2, defined as follows:

$$\left(\frac{\Delta P_f}{\Delta Z}\right)_{TP} = \phi_L^2 \left(\frac{\Delta P_f}{\Delta Z}\right)_L, \tag{26}$$

where $(\Delta P_f/\Delta Z)_L$ is the frictional pressure drop when liquid is assumed to flow alone in the channel. The friction multiplier has been correlated in terms of the Lockhart–Martinelli parameter, X, given by

$$X^2 = \frac{(\Delta P_f/\Delta Z)_L}{(\Delta P_f/\Delta Z)_G}, \tag{27}$$

where $(\Delta P_f/\Delta Z)_G$ is the frictional pressure drop when the gas is assumed to flow alone in the channel. A widely used correlation to calculate the friction multiplier is that proposed by Chisholm and Laird (1958),

$$\phi_L^2 = 1 + \frac{C}{X} + \frac{1}{X^2}, \tag{28}$$

where the coefficient, C, is a constant ranging in value from 5 to 20 for larger channels, depending on whether the liquid and gas are laminar or turbulent. For the present two-phase flow conditions in a microchannel, the value of C would be 5 because both the liquid and gas flows are laminar, i.e., $Re_L(= G_L D_H/\eta_L) < 2000$ and $Re_G(= G_G D_H/\eta_G) < 2000$.

The C-value in Eq. (28) is known to decrease as the channel hydraulic diameter is reduced (Kawaji, 1999), and Mishima and Hibiki (1996) have proposed a correlation for the C-value for small diameter channels as follows:

$$C = 21(1 - e^{-0.319 D_H}). \tag{29}$$

Eq. (29) was developed using the available air–water two-phase flow data obtained in circular and rectangular channels with $D_H = 1$–4 mm.

Recently, Lee and Lee (2001a) measured pressure drop for air–water two-phase flows in horizontal rectangular channels with a small height and having a hydraulic diameter, $D_H = 0.78$ to 6.67 mm. They proposed the following correlation for the C-value based on their own data:

$$C = A\lambda^q \psi^r Re_{LO}^s, \tag{30}$$

where Re_{LO} is the liquid Reynolds number when the total mass flux is assumed to be that of liquid alone,

$$Re_{LO} = \frac{G D_H}{\eta_L}. \tag{31}$$

The dimensionless parameters, λ and ψ were defined as

$$\lambda = \frac{\eta_L^2}{\rho_L \sigma D_H} \tag{32}$$

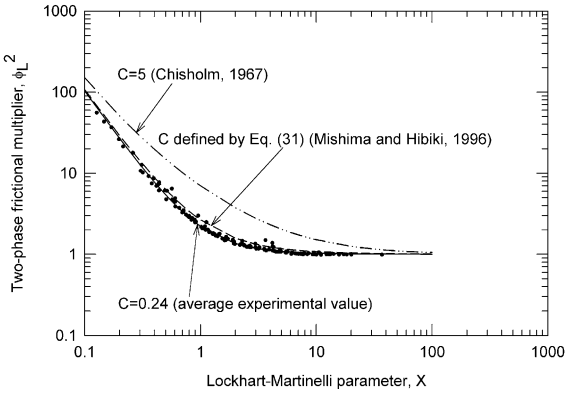

Fig. 14. Variation of two-phase friction multiplier data with Lockhart–Martinelli parameter.

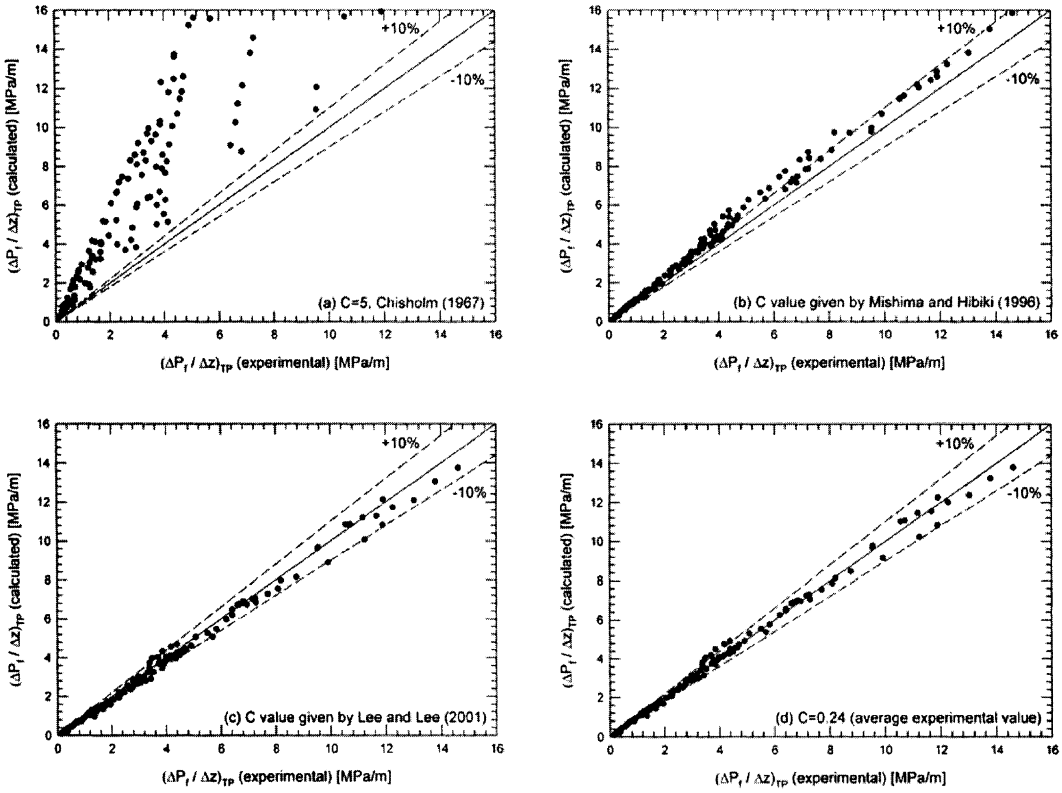

Fig. 15. Predictions of two-phase friction pressure gradient data by a Lockhart–Martinelli correlation with different C-values.

and

$$\psi = \frac{\eta_L j}{\sigma}, \tag{33}$$

where σ is the surface tension and j the total superficial velocity ($= j_G + j_L$). The values of A, q, r and s in Eq. (30) depend on whether the liquid and gas are laminar or turbulent.

Fig. 14 shows a comparison of the two-phase friction multiplier data with the values predicted by Eq. (28) with $C = 5$, as recommended by Chisholm and Laird (1958) for both phases being laminar, and with $C = 0.66$ given by Mishima and Hibiki's (1996) correlation. It is clear that the data can be correlated well using a Lockhart–Martinelli parameter, but the predictions of Eq. (28) with $C = 5$ are well over the present data. On the other hand, the friction multiplier values calculated with $C = 0.66$ are slightly higher than the experimental data, while a slightly smaller value of $C = 0.24$ was found to best fit the present results.

Finally, a comparison of the two-phase frictional pressure gradient data with the predictions of the Lockhart–Martinelli correlation using different C-values is shown in Fig. 15, including $C = 5$, $C = 0.66$ from Eq. (29), C calculated from Lee and Lee's model (Eq. (30)), and $C = 0.24$. The conventional value of $C = 5$ again significantly over-predicted the present data, while Mishima & Hibiki's correlation generally over-predicted the data by about 10%. On the other hand, good agreement (within $\pm 10\%$) was obtained with the use of the C-value given by Lee and Lee's model and the present value of $C = 0.24$.

4. Conclusions

An experimental investigation has been carried out on two-phase flow characteristics in a 100 μm diameter circular tube using de-ionized water and nitrogen gas. Two-phase flow patterns, time-averaged void fraction and two-phase frictional pressure drop data were measured and analyzed. Based on the results presented, the following conclusions can be presented:

(1) The two-phase flow patterns observed were mainly intermittent and semi-annular flows, but a closer study of the liquid film structure revealed gas core flows with a smooth or ring-shaped film and a serpentine-like gas core flow surrounded by a deformed liquid film. Bubbly flow was not observed in the present work, even at the highest superficial liquid velocity ($j_L \sim 4$ m/s) and lowest superficial gas velocity ($j_G \sim 0.1$ m/s) tested.
(2) The probability of appearance of different flow patterns revealed a gradual shift in the predominant flow pattern with increasing gas and liquid flow rates. For low liquid flow rates, gas core flows with a smooth-thin liquid film occurred most frequently at low gas flow rates, but gas core flows with a ring-shaped liquid film became more frequent at high gas flow rates. At high liquid flow rates, gas core flows with a thick liquid film, and serpentine-like gas core flows with a deformed liquid film also appeared. At high gas and liquid flow rates, all types of gas core flows appeared, and this was named a multiple flow pattern.
(3) A flow pattern map was developed based on the probability of appearance of each flow type, and compared to existing flow pattern maps obtained from ~1-mm diameter channels. Similarities and differences between the microchannel and larger diameter tubes were identified. The absence of bubbly and churn flow patterns in the microchannel results was attributed to the low liquid Reynolds numbers and laminar nature of liquid flow in the present microchannel because of the small channel diameter.

(4) Time-averaged void fraction data were obtained from the analysis of two-phase flow images captured at different flow rates. The time-averaged void fraction remained low even at high gas flow rates, indicating significantly larger slip ratios and weaker momentum coupling between the phases, compared to the flows in channels with $D_H \sim 1$ mm. This was consistent with the occurrence of predominantly liquid-only or separated flow patterns in the microchannel.
(5) Single-phase friction factor and two-phase friction multiplier data were obtained from the pressure drop data. The single-phase friction factor was shown to be in good agreement with the conventional laminar correlation. The two-phase friction multiplier data were over-predicted by the homogeneous flow model, but correlated well (within $\pm 10\%$) with the separated flow model of Lockhart and Martinelli (1949).

Acknowledgements

The authors wish to thank the Natural Sciences and Engineering Research Council of Canada for financially supporting the present work through a Research Grant and an Equipment Grant. The authors are also grateful to the Government of Ontario (a graduate student scholarship for P.M.-Y. Chung) and the Japanese Ministry of Education, Culture, Sports, Science and Technology (a fellowship for A. Kawahara).

References

Ali, M.I., Sadatomi, M., Kawaji, M., 1993. Two-phase flow in narrow channels between two flat plates. Can. J. Chem. Eng. 71, 657–666.

Armand, A.A., 1946. The resistance during the movement of a two-phase system in horizontal pipes, Izv. Vses. Teplotekh. Inst., 1, 16-23 (AERE-Lib/Trans 828).

Beattie, D.R.H., Whalley, P.B., 1982. A simple two-phase flow frictional pressure drop calculation method. Int. J. Multiphase Flow 8, 83–87.

Chen, I.Y., Yang, K.S., Chang, Y.J., Wang, C.C., 2001. Two-phase pressure drop of air–water and R-410A in small horizontal tubes. Int. J. Multiphase Flow 27, 1293–1299.

Chisholm, D., 1983. Two-phase flow in pipelines and heat exchangers. Pitman Press, Bath, England.

Chisholm, D., Laird, A.D.K., 1958. Two-phase flow in rough tubes. Trans. ASME 80 (2), 276–286.

Cicchitti, A., Lombardi, C., Silvestri, M., Solddaini, G., Zavalluilli, R., 1960. Two-phase cooling experiments—Pressure drop, heat transfer and burnout measurement. Energia Nucl. 7 (6), 407–425.

Collier, J.G., 1972. Convective Boiling and Condensation. McGraw-Hill Book Co, UK.

Coleman, J.W., Garimella, S., 1999. Characterization of two-phase flow patterns in small diameter round and rectangular tubes. Int. J. Heat Mass Transfer 42, 2869–2881.

Damianides, C.A., Westwater, J.W., 1988. Two-phase flow patterns in a compact heat exchanger and small tubes. In: Proceedings of Second UK National Conference on Heat Transfer, Glasgow, September 14–16. Mechanical Engineering Publications, London, pp. 1257–1268.

Dukler, A.E., Wicks III, M., Cleveland, R.G., 1964. Pressure drop and hold-up in two-phase flow. AIChE J. 10 (1), 38–51.

Feng, Z.P., Serizawa, A., 1999. Visualization of two-phase flow patterns in an ultra-small tube. In: Proceedings of the 18th Multiphase Flow Symposium of Japan, Suita, Osaka, Japan, July 15–16, pp. 33–36.

Feng, Z.P., Serizawa, A., 2000. Measurement of steam-water bubbly flow in ultra-small capillary tube. In: Proceedings of the 37th National Heat Transfer Symposium of Japan, vol. I, pp. 351–352.

Fukano, T., Kariyasaki, A., 1993. Characteristics of gas–liquid two-phase flow in a capillary. Nucl. Eng. Des. 141, 59–68.

Garimella, S., Killion, J.D., Coleman, J.W., 2001. An experimental validated model for two-phase pressure drop in the intermittent flow regime for circular microchannels. In: Proceedings of ASME NHTC'01 35th National Heat Transfer Conference, Anaheim, California, p. 12.

Hewitt, G.F., Shires, G.L., Bott, T.R., 1993. Process Heat Transfer. CRC Press, Ann Arbor, Michigan.
Ho, C.-M., Tai, Y.-C., 1998. Micro-electro-mechanical-systems (MEMS) and fluid flows. Annu. Rev. Fluid Mech. 30, 579–612.
Ide, H., Matsumura, H., Tanaka, Y., Fukano, T., 1997. Flow patterns and frictional pressure drop in gas–liquid two-phase flow in vertical capillary channels with rectangular cross-section. Trans. JSME 63, 452–460.
Joseph, D.D., Bai, R., Chen, K.P., Renardy, Y.Y., 1997. Core-Annular Flows. Annu. Rev. Fluid Mech. 29, 65–90.
Kawaji, M., 1999. Fluid mechanics aspects of two-phase flow: Flow in other geometries. In: Kandlikar, S.G., Shoji, M., Dhir, V.K. (Eds.), Handbook of Phase Change: Boiling and Condensation. Taylor & Francis, Washington, DC, pp. 205–259.
Kawaji, M., Chung, P.M.-Y., Kawahara, A., 2001. Instantaneous velocity profiles and characteristics of pressure-driven flow in microchannels. In: Proceedings of 2001 ASME IMECE, November 11–16, 2001, New York, pp. 1–11.
Keska, J.K., Fernando, R.D., 1994. Average physical parameters in an air–water two-phase flow in a small square-sectioned channel. J. Fluids Eng.—Trans. ASME 116, 247–256.
Lee, H.J., Lee, S.Y., 2001a. Pressure drop correlations for two-phase flow within horizontal rectangular channels with small height. Int. J. Multiphase Flow 27, 783–796.
Lee, H.J., Lee, S.Y., 2001b. Heat transfer correlation for boiling flows in small rectangular horizontal channels with low aspect ratios. Int. J. Multiphase Flow 27, 2043–2062.
Lin, S., Kew, P.A., Cornwell, K., 1999. Characteristics of air/water flow in small tubes. Int. J. Heat Technol. 17 (2), 63–70.
Lin, S., Kwok, C.C.K., Li, R.Y., Chen, Z.H., Chen, Z.Y., 1991. Local frictional pressure drop during vaporization for R-12 through capillary tubes. Int. J. Multiphase Flow 17, 95–102.
Lockhart, R.W., Martinelli, R.C., 1949. Proposed correlation of data for isothermal two-phase, two-component flow in pipes. Chem. Eng. Progress 45, 39–48.
McAdams, W.H., 1954. Heat Transmission, third ed. McGraw-Hill, New York.
Mishima, K., Hibiki, T., 1996. Some characteristics of air–water two-phase flow in small diameter vertical tubes. Int. J. Multiphase Flow 22 (4), 703–712.
Owens, W.L., 1961. Two-phase pressure gradient. Int. Dev. in Heat Transfer, Pt II. ASME, New York.
Schmidt, F.W., Zeldin, B., 1969. Laminar flows in tubes and ducts. AIChE J. 6 (15), 612–614.
Serizawa, A., Feng., Z.P., 2000. Review of two-phase flow in micro-channels. In: Proceedings of The US-Japan Seminar on Two-Phase Flow Dynamics, June 4–9, 2000, Santa Barbara, USA, pp. 429–451.
Serizawa, A., Feng, Z.P., 2001. Two-phase flow in micro-channels. In: Proceedings of the 4th International Conference on Multiphase Flow, May 27–June 1, 2001, New Orleans, LA, USA.
Stanley, R.S., Barron, R.F., Ameel, T.A., 1997. Two-phase flow in microchannels. Micro-Electro-Mechanical Systems (MEMS), ASME, DSC-Vol. 62/HTD-Vol. 354.
Suo, M., Griffith, P., 1964. Two-phase flow in capillary tubes. J. Basic Eng. 86, 576–582.
Triplett, K.A., Ghiaasiaan, S.M., Abdel-Khalik, S.I., LeMouel, A., McCord, B.N., 1999a. Gas–liquid two-phase flow in microchannels. Part II: void fraction and pressure drop. Int. J. Multiphase Flow 25, 395–410.
Triplett, K.A., Ghiaasiaan, S.M., Abdel-Khalik, S.I., Sadowski, D.L., 1999b. Gas–liquid two-phase flow in microchannels—Part I: Two-phase flow pattern. Int. J. Multiphase Flow 25, 377–394.
Ungar, E.K., Cornwell, J.D., 1992. Two-phase pressure drop of ammonia in small diameter horizontal tubes. AIAA 17th Aerospace Ground Testing Conf., Nashville, TN, July 6–8.
Wong, T.N., Ooi, K.T., 1995. Refrigerant flow in capillary tube: An assessment of the two-phase viscosity correlations on model. Int. Comm. Heat Mass Transfer 22 (4), 595–604.
Xu, J.L., Cheng, P., Zhao, T.S., 1999. Gas–liquid two-phase flow regimes in rectangular channels with mini/micro gaps. Int. J. Multiphase Flow 25 (3), 411–432.
Yang, C-Y., Shieh, C-C., 2001. Flow pattern of air–water and two-phase R-134a in small circular tubes. Int. J. Multiphase Flow 27 (7), 1163–1177.
Zhao, T.S., Bi, Q.C., 2001a. Co-current air–water two-phase flow patterns in vertical triangular microchannels. Int. J. Multiphase Flow 27, 765–782.
Zhao, T.S., Bi, Q.C., 2001b. Pressure drop characteristics of gas–liquid two-phase flow in vertical miniature triangular channels. Int. J. Heat Mass Transfer 44, 2523–2534.